Proc. Natl. Acad. Sci. USA
Vol. 95, pp. 8034–8039, July 1998
Biophysics

Myosin conformational states determined by single fluorophore polarization

DAVID M. WARSHAW*†, ERIC HAYES*, DONALD GAFFNEY*, ANNE-MARIE LAUZON*, JUNRU WU‡, GUY KENNEDY§, KATHLEEN TRYBUS¶, SUSAN LOWEY¶, AND CHRISTOPHER BERGER*

Departments of *Molecular Physiology and Biophysics, ‡Physics, and the §Instrumentation and Model Facility, University of Vermont, Burlington, VT 05405; and ¶Brandeis University, Rosenstiel Basic Sciences Research Center, Waltham, MA 02254

Edited by Thomas D. Pollard, The Salk Institute for Biological Studies, La Jolla, CA, and approved May 8, 1998 (received for review March 19, 1998)

ABSTRACT **Muscle contraction is powered by the interaction of the molecular motor myosin with actin. With new techniques for single molecule manipulation and fluorescence detection, it is now possible to correlate, within the same molecule and in real time, conformational states and mechanical function of myosin. A spot-confocal microscope, capable of detecting single fluorophore polarization, was developed to measure orientational states in the smooth muscle myosin light chain domain during the process of motion generation. Fluorescently labeled turkey gizzard smooth muscle myosin was prepared by removal of endogenous regulatory light chain and re-addition of the light chain labeled at cysteine-108 with the 6-isomer of iodoacetamidotetramethylrhodamine (6-IATR). Single myosin molecule fluorescence polarization data, obtained in a motility assay, provide direct evidence that the myosin light chain domain adopts at least two orientational states during the cyclic interaction of myosin with actin, a randomly disordered state, most likely associated with myosin whereas weakly bound to actin, and an ordered state in which the light chain domain adopts a finite angular orientation whereas strongly bound after the powerstroke.**

At the molecular level, muscular force and motion generation are the result of a cyclic interaction between myosin and actin. The energy required to drive this mechanical process is derived from the hydrolysis of MgATP by myosin. Forty years ago, A. F. Huxley proposed a simple two-state model of force generation in which myosin undergoes a transition between a detached and an attached state to actin (1). This two-state model was later supported by evidence demonstrating that myosin biochemically undergoes a weak to strong binding transition (2, 3), which could be conformationally described through EPR spectroscopic studies as a disordered to ordered transition (4). Implicit in these models is that, although myosin is strongly bound to actin, it must undergo a powerstroke to generate force and motion. Based on ultrastructural, EPR, x-ray diffraction (for review, see ref. 5), and more recent crystallographic data (6, 7), detailed models have been proposed to describe conformational states of myosin during the crossbridge cycle and how myosin domains may be involved in the powerstroke (5, 7, 8).

Myosin S1 is an asymmetric molecule having a globular catalytic domain that contains the hydrolytic and motor activities of myosin and a light chain domain that consists of an 8.5-nm α-helix, which is stabilized by an essential and regulatory light chain (RLC) (see Figs. 2 and 5). It is now believed that during the powerstroke, the catalytic domain remains attached to actin in a fixed orientation and that the light chain domain acts as a rigid lever arm to amplify small conformational changes originating in the catalytic domain (for review, see ref. 9). Early support for this type of model (5) came from EPR experiments showing that probes on the catalytic domain have only a distinct single orientation during muscle contraction (4). Further support for a fixed catalytic and "swinging" light chain domain have been recently obtained from both fluorescence polarization (10–13) and EPR (14) data in skinned muscle fibers. However, any proposed model for myosin conformational states during the crossbridge cycle (e.g., disordered to ordered) and the powerstroke itself all have been obtained from studies of myosin populations, whether it be in the test tube or the muscle fiber. For example, during force production, any observed myosin conformational changes within a fiber are the average for the entire myosin population, many of which may not contribute to force production. Specifically, a significant fraction of the myosin population ($\approx$80%) during isometric force production is weakly bound to actin and presumably disordered (4, 15), whereas the remaining strongly bound, ordered force-generating population are distributed amongst mechanical states associated with different steps in the actomyosin cycle. To avoid the complexities associated with population-based myosin studies, we have developed a spot-confocal fluorescence microscope (16) capable of detecting single fluorophore polarization, with the goal of measuring single myosin molecule conformational states during the crossbridge cycle in the *in vitro* motility assay. By measuring fluorescence polarization from single smooth muscle myosin molecules, with fluorescently labeled RLC, we have obtained direct real-time evidence that a myosin molecule does in fact undergo a disordered to ordered transition when going from a detached to attached force-generating state, as suggested by EPR studies (4, 14).

METHODS

Protein Preparation. Thiophosphorylated turkey gizzard smooth muscle myosin and actin were prepared by standard methods as stated in Trybus *et al.* (17). Smooth muscle RLC was expressed in *Escherichia coli* and purified as outlined in Trybus and Chatman (18). Endogenous RLC was removed from smooth muscle myosin by gel filtration on a column containing trifluoperazine (17). The RLC-deficient myosin was reconstituted with thiophosphorylated RLC that had been labeled at cysteine-108 with the 6-isomer of iodoacetamidotetramethylrhodamine (6-IATR), using the labeling methods described (10); $\approx$50% labeling was achieved. Comparison of *in*

The publication costs of this article were defrayed in part by page charge payment. This article must therefore be hereby marked "*advertisement*" in accordance with 18 U.S.C. §1734 solely to indicate this fact.

This paper was submitted directly (Track II) to the *Proceedings* office.
Abbreviations: 6-IART, 6-isomer of iodoacetamidotetramethylrhodamine; SAPD, silicon avalanche photodiode detectors; RLC, regulatory light chain.
†To whom reprint requests should be addressed. e-mail: warshaw@salus.med.uvm.edu.

vitro motility for both unlabeled control and labeled myosin suggested that the incorporation of labeled RLC had no deleterious effects on the mechanical performance of myosin.

Motility and Laser Trap Assays. Fluorescently labeled myosin was studied in an *in vitro* motility assay by adhering it to a nitrocellulose-coated coverslip, which was part of a microchamber placed on the stage of a spot-confocal fluorescence microscope (Fig. 1). In this assay, fluorescently labeled myosin could interact with actin filaments in the presence or absence of MgATP. The general methods for preparing the nitrocellulose-coated coverslips and microchamber flow cells have been described (19). The experiments were performed as follows. A desired mixture of unlabeled and 6-IATR-labeled myosin in myosin buffer (25 mM Imidazole/300 mM KCl/1 mM EGTA/4 mM $MgCl_2$/10 mM DTT, pH 7.4) was added to the 15-μl microchamber and allowed to adhere to the nitrocellulose surface for 1 min. The myosin was then flushed from the microchamber with 30 μl of BSA (0.5% BSA in myosin buffer). After the BSA wash, the microchamber was flushed with actin buffer [25 mM Imidazole/300 mM KCl/1 mM EGTA/4 mM $MgCl_2$/10 mM DTT plus oxygen scavengers from Fluka (0.1 mg/ml glucose oxidase/0.018 mg/ml catalase/2.3 mg/ml glucose), pH 7.4] to wash away excess BSA and promote actin binding to the myosin on the nitrocellulose surface. After this, 15 μl of coumarin–phalloidin-labeled actin [10 nM] in actin buffer was added and allowed to interact with the myosin for 1 min. An excess of unlabeled actin [10 μM] in actin buffer with 0.5% methylcellulose and the desired concentration of MgATP was added to the microchamber. The coumarin–actin could be visualized by a SIT camera and was used as a marker for the focal plane of the myosin surface. The excess unlabeled actin was used to maximize the chance that a myosin molecule would be interacting with an actin filament. The concentration of unlabeled actin was 2,000 times greater than normally used in the motility assay. Once the coumarin–actin was visualized, the Hg lamp that excited the coumarin label was shuttered off whereas the Argon laser, used to excite the 6-IATR-labeled RLC was simultaneously shuttered on. Fluorescence intensity was then photon counted by silicon avalanche photodiodes as described below.

In a separate set of experiments, smooth muscle heavy meromyosin was studied in a laser optical trap (20, 21) in an effort to measure unitary displacement events and their duration under identical ionic conditions and [MgATP] as were

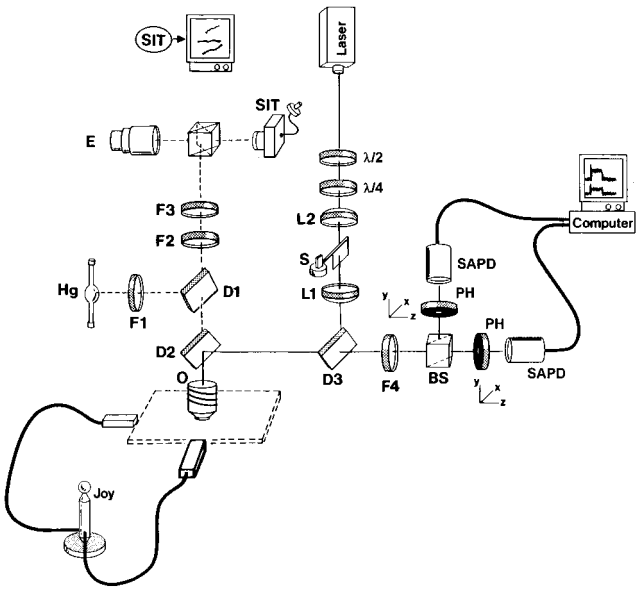

FIG. 1. Fluorescence detection system. Spot-confocal microscope block diagram (see text for description).

the fluorescently labeled myosins in the motility assay described above. These experiments were performed to confirm that the fluorescence polarization events were in fact indicative of myosin conformational states during motion generation. The procedures and instrumentation have been described in detail previously (20, 21) and were identical to that used in this study. Laser trap-displacement event durations were determined by mean-variance analysis as described in Guilford *et al.* (20). Event durations were obtained for smooth muscle heavy meromyosin at both 1 and 10 μM MgATP.

Spot Confocal Fluorescence Microscope and Polarization Detection. The single rhodamine fluorophore detection system was composed of an Argon laser (Spectra-Physics; Model 163-C0201) used to excite the 6-IATR probe with 9 mW of 514 nm light originating from the laser. Given that myosin molecules on the coverslip will be randomly oriented, so too will be the individual rhodamine absorption dipoles. Therefore, by using circularly polarized laser light, the probability of exciting any given fluorophore is maximized. To attain circular polarization at the motility surface, the linear polarized light from the laser passed through a $\lambda/2$ and then a $\lambda/4$ waveplate. The light then entered a 2X beam expander (L1,L2) and reflected off of two dichroic mirrors (D3,D2) before filling the back aperture of the objective (O) (Zeiss; Neofluoror 100X, numerical aperture = 1.3) on a upright microscope (Zeiss; Lab Standard), to create a diffraction limited spot ($\approx$0.5 μm diameter) on the motility surface. When a manual shutter (S) allowed the laser excitation to enter the microscope, rhodamine epifluorescence was then reflected by D2 (pass $<$450 nm and $>$625 nm, reflect 500–625 nm; Chroma Technology, Brattleboro, VT) through D3 and barrier filtered (F4) (D3,F4 components of a High Q TRITC filter set; Chroma Technology) before being split into its orthogonal x- and y-polarized components (i.e., I_x, I_y) by a polarizing beam splitter (BS). The x- and y-components passed through 75-μm diameter pinholes (PH; Melles Griot, Irvine, CA) to reject out of focus light before detection by photon-counting silicon avalanche photodiode detectors (SAPD; EG & G Optoelectronics, Quebec, Canada; SPCM-200-PQ). The SAPD outputs were digitized by multichannel scalar cards (EG & G Ortec, Oak Ridge, TN; MCS-Plus) in a 386 laboratory computer.

To visualize individual actin filaments labeled with coumarin–phalloidin, light from a 100-W Hg lamp was used to excite the coumarin emission through a filter set (F1, D1, F2; CZ-702 Filter set; Chroma Technology). Before the coumarin fluorescence entered a SIT camera (Dage–MTI, Michigan City, IN; Model 66), the light was bandpass filtered (F3; 440 nm/40 nm) to eliminate any laser light. The SIT camera image was digitally processed (Hamamatsu, Bridgewater, NJ, Argus 10) to enhance the actin filament image.

A custom joystick-controlled micromanipulated microscope stage was constructed by using actuators from a Narishige micromanipulator (East Meadow, NY, MW-2). The experiments were performed at 25°C by using a custom objective heater.

The fluorescence emission intensity, I_{xy}, that is detected in the x-y plane by the SAPDs as a result of the emission dipole electric field vector E is defined as: $I_{xy} = I \sin^2 \theta = I_x + I_y$ and also is related to the fluorescence polarization angle ϕ as follows: $\cos^2\phi = I_x/(I_x + I_y)$ (see Fig. 2 for symbol definitions). The ϕ reported here was determined by this relationship. It is assumed that fluorophore is rigidly adhered to the RLC on the time scale of the fluorescence lifetime. In addition, the accuracy of this estimate of ϕ was confirmed by independently calibrating the detection system by using polarized light generated by passing light from an incandescent bulb through a polarizer (Mells Griot) on the microscope stage. The polarized light then entered the objective and was detected by the SAPDs and used to determine the relationship between total intensity and polarization angle. As defined by this spatial

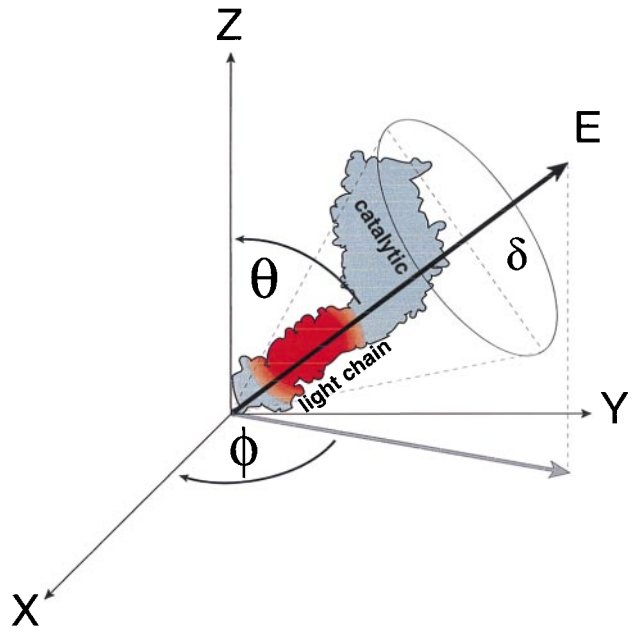

FIG. 2. Spatial model for fluorophore emission dipole. A myosin molecule is illustrated (only the S1 subfragment is depicted with the catalytic and light chain domains labeled), adhered to the plane of the motility surface (x-y plane). The emission dipole electric field vector (E), associated with the 6-IATR-labeled RLC in the myosin light chain domain, is defined in space by its angle, ϕ, in the x-y plane and angle, θ, relative to the z-axis. The wobble cone for the fluorophore is defined by angle δ, although we have assumed that the fluorophore is rigidly adhered to the RLC.

model, observed increases in total fluorescence intensity can be obtained if the emission dipole swings away from the z-axis (i.e., for θ approaching 90°).

RESULTS AND DISCUSSION

To verify that the microscope system was capable of resolving single fluorophores, a mixture of unlabeled and 6-IATR-labeled myosin was adhered to the coverslip surface in the absence of MgATP. The concentration of labeled myosin in the mixture (total myosin = 200 μg/ml) was varied between 0.001–100 μg/ml. The high total myosin concentration for the mixture was needed to ensure that actin filaments would remain on the surface and thus interact with myosin (see *Methods*). Shown in Fig. 3*A* are the fluorescence emission time courses for coverslip surfaces with 0, 0.5, 1.0, and 10 μg/ml-labeled myosin within the mixture. At labeled myosin concentrations >10 μg/ml, the density of fluorophores was sufficiently high to demonstrate an exponential decay of fluorescence intensity caused by photobleaching. However, at ≤1.0 μg/ml-labeled myosin, the fluorophore density was now limiting so that photobleaching was quantal, indicative of a single fluorophore (22–26). The log of peak photon counts for the y-polarized fluorescence emission is plotted against the log of the labeled myosin concentration on the coverslip surface. The peak fluorescence intensity was linearly related to the labeled myosin concentration until the point in which further dilutions of the labeled myosin had no effect on fluorescence intensity and in which the intensity was similar to control, i.e., where only unlabeled myosin was adhered to the surface.

To estimate the number of labeled myosin molecules within the laser excitation spot, we used a previously determined relationship between the myosin concentration added to the experimental chamber and the resultant surface density of adherent myosin molecules (27). Based on this estimate, the breakpoint in the relationship between peak fluorescence intensity and labeled myosin concentration occurs between 0.7 and 1.4 labeled myosin molecules (see Fig. 3*B*). The myosin concentration used in the laser trap studies (20) to ensure recordings from a single myosin molecule (i.e., 0.5–2 μg/ml) is identical to that needed to observe single fluorophores. These results support our capacity to detect single fluorophores by using a similar detection system described by Nie *et al.* (16).

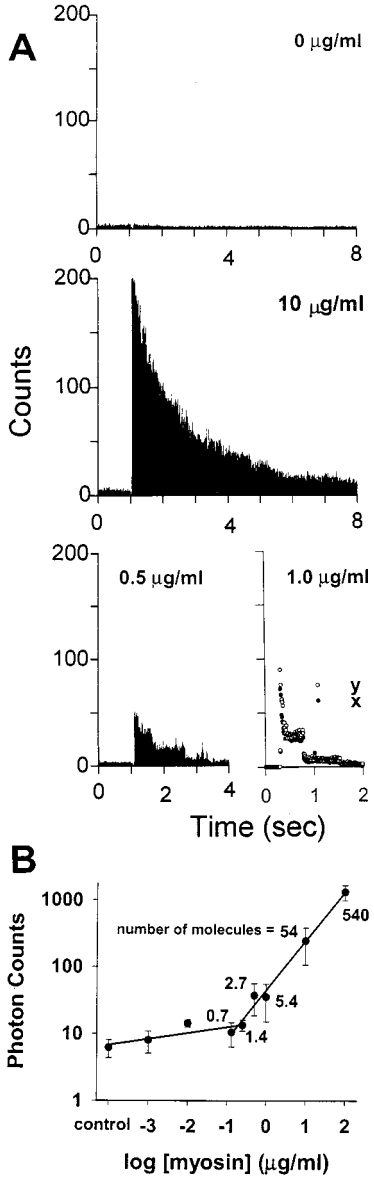

FIG. 3. Fluorescence emission intensity vs. 6-IATR-labeled myosin concentration on the motility surface. (*A*) Only the y-polarized fluorescence from a mixture of labeled and unlabeled myosin on the motility surface is shown at 1-ms integration rate for mixtures containing 0, 0.5, 1.0, and 10 μg/ml of labeled myosin. The peak fluorescence of 248 counts at 10 μg/ml labeled myosin is not shown so that the ordinate could be the same for all traces. At 0.5 μg/ml-labeled myosin, quantal photobleaching events are apparent. A more detailed view of unitary photobleaching events for both the x- (○) and y-polarized (●) emission at 1.0 μg/ml-labeled myosin in the mixture is shown. (*B*) The log of peak fluorescence emission intensity vs. the log of labeled myosin concentration in the myosin surface mixture plotted with linear regressions through the data between 0 and 0.25 μg/ml and between 0.13 and 100 μg/ml. Data points are presented as the mean (●) and standard error for at least seven measurements per concentration. The numbers next to the data points are the estimated number of labeled myosin molecules that exist in the excitation spot based on previous myosin surface density estimates (27).

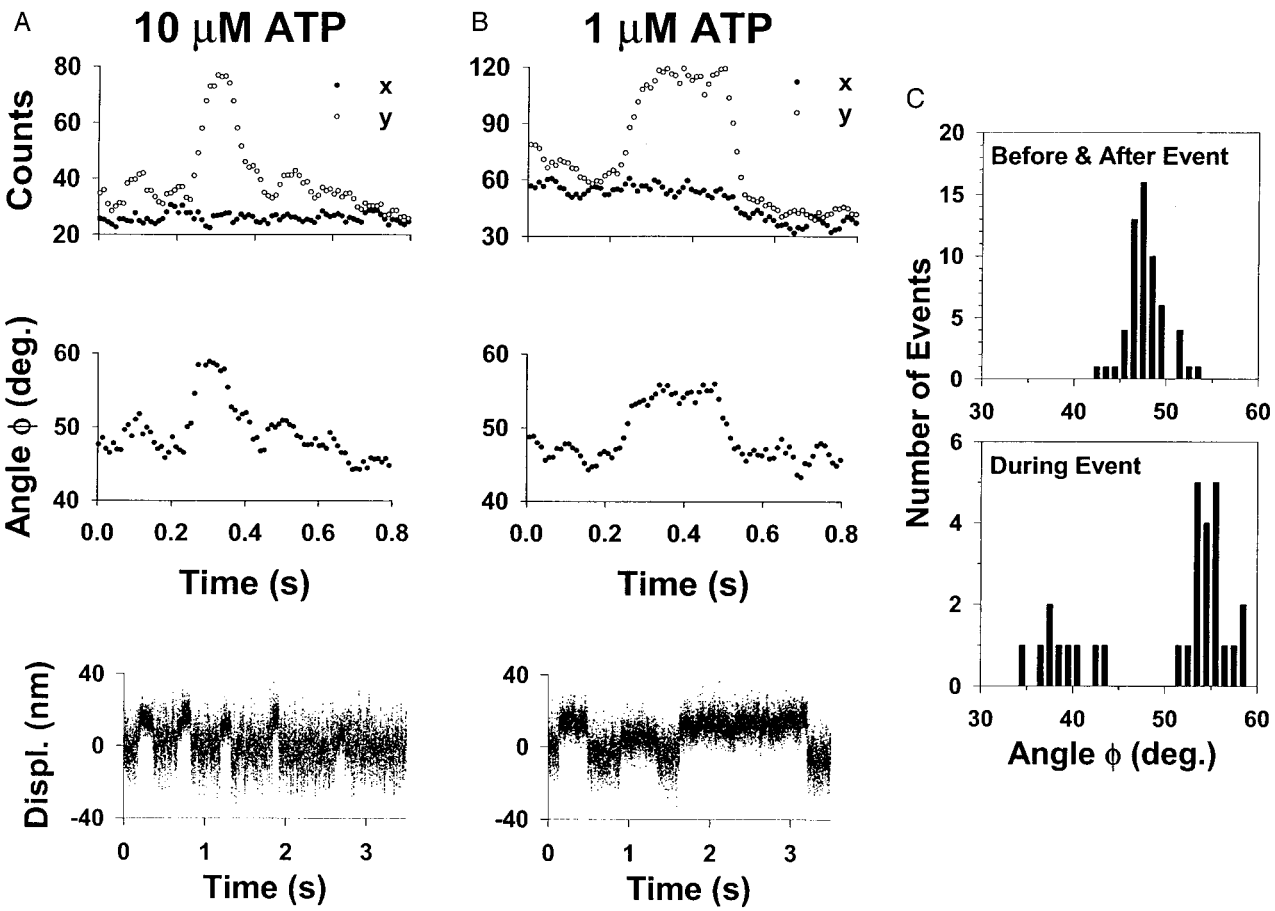

FIG. 4. Fluorescence polarization and unitary displacements as function of MgATP concentration and polarization angle histograms. (*A Top* and *B Top*) Examples of x- and y-polarized fluorescence emission signals initially collected at a 1-ms integration rate then resampled at a 10-ms rate and filtered by using a five-point moving average for 10 μm and 1 μM MgATP. (*A Middle* and *B Middle*) The x-y plane projected emission dipole polarization angles (ϕ) determined from the fluorescence emission signals in the traces above by using the equations in *Methods*. (*A Bottom* and *B Bottom*) Representative unitary displacement records from smooth muscle heavy meromyosin obtained under similar experimental conditions as in the fluorescence polarization experiment, using the laser optical trap. See Guilford *et al.* (20) for experimental details. Myosin generated displacements of ≈10 nm are seen as upward deflections in the traces. (*C* Histograms of the average ϕ determined both 100 ms before and after the polarization event (*Upper*) and during the event (*Lower*).

Only in the presence of MgATP and actin were transient changes in the x- and y-polarized emission observed from fluorescently labeled myosin (see Fig. 4 *A Top* and *B Top*). To relate these polarization events to angular changes in the fluorophore emission dipole, we assumed a spatial model for the attachment of 6-IATR-labeled myosin to the motility surface (see Fig. 2). Given our detection plane, any observed fluorescence from the emission dipole will only be a two-dimensional projection onto the plane of the microscope stage (i.e., the plane of the orthogonal x- and y-polarized components). Note that any motion of the fluorophore that is limited to a plane perpendicular to the x-y plane, i.e., a change in θ only (Fig. 2), would be detected as a change in the overall intensity ($I_x + I_y$) and thus a simultaneous change of equal proportion in both x- and y-polarizations. Polarization events described by such a change were not scored because of the potential that an artifact, such as a dust particle crossing the excitation or emission light paths, would give similar results.

Polarization transients, which were scored by visual detection, occurred on an intensity signal that photobleached to baseline in a single step, thus ensuring a response from a single fluorophore. These transients were characterized by total intensity changes that were step-like, with most of the intensity change occurring in either the x- or y-polarization channel (see Fig. 4). The fact that transient polarization events were not described by intensity changes in the x- and y-polarization channels that were opposite in direction, suggests that motions of the fluorophore in only the x-y plane rarely occur. This result can be explained if myosin only supports actin filament motility when the light chain domain and thus the powerstroke swing angle occurs in a plane other than the motility surface (i.e., the x-y detection plane). Therefore, motion of the emission dipole along this swing angle would result in polarization transients of the type that we observed, where transients were described both by a total intensity change resulting from the dipole moving toward or away from the *z*-axis (θ) and by a polarization change in the x-y plane (ϕ).

If the observed polarization events are related to the myosin powerstroke, then the polarization event duration should be dependent on MgATP concentration. Without MgATP, step polarization transients were not observed. At 10 μM MgATP, event durations lasted ≈200 ms, increasing to ≈400 ms at 1 μM MgATP (see Table 1). If this prolongation at limiting [MgATP] is caused by the myosin waiting for the next MgATP to bind after completion of the powerstroke, then the MgATP dependence for the polarization events should be similar to single smooth muscle myosin molecule-displacement event durations measured in the laser optical trap under unloaded conditions (20). Therefore, laser trap experiments were performed by using smooth muscle heavy meromyosin under similar ionic conditions as were the polarization experiments. As seen in Fig. 4 and Table 1, the durations and MgATP dependence of the polarization and unitary displacement events are remarkably similar, providing evidence that both

Table 1. Comparison of event durations obtained from fluorophore polarization, laser trap displacement, and biochemical rate constants

	Event durations, ms	
[MgATP]	10 μM	1 μM
Fluorophore polarization	187 ± 14 (n = 15)	376 ± 30 (n = 13)
Laser trap unitary displacements*	158 ± 19 (n = 12)	505 ± 77 (n = 6)
Biochemical model†	≈120	≈570

*Estimates of event durations obtained by mean-variance analysis of single myosin molecule displacement records in the laser optical trap (see ref. 20 for details) under identical ionic and experimental conditions used in the fluorescence polarization experiments.

†Using rate constants from solution studies of the actomyosin ATPase cycle (28), for MgADP release (≈15 s^{-1}) and for MgATP binding and subsequent myosin detachment from actin (≈2 × 10^6 M^{-1} s^{-1}), one can calculate the total time associated with MgADP release, MgATP binding, and myosin detachment, i.e., presumably the duration of the powerstroke.

are derived from the myosin powerstroke. As further support, if one assumes that the unitary polarization and displacement events relate to the period of time that myosin is strongly bound to actin, then one can estimate the event duration from enzyme kinetic data. Assuming that the strongly bound time is limited both by the rate of MgADP release (≈15 s^{-1}) and the subsequent MgATP binding to the smooth muscle myosin active site (≈2 × 10^6 M^{-1} s^{-1}), then estimated event durations based on these biochemical rates (28) of ≈120 ms at 10 μM MgATP and ≈570 ms at 1 μM MgATP agree well with both the polarization and displacement event durations (see Table 1).

The polarization events, as seen in Fig. 4, suggest that the fluorophore emission dipole adopts an orientation during the event that differs from that both before and after the event. The average polarization angle, both before and after an event, clustered about a mean of ϕ = 48° (Fig. 4*C Upper*). This angle might indicate a preferred orientation of the myosin molecule on the motility surface. However, it is more likely that the fluorophore, the myosin light chain domain, or the myosin molecule itself has significant rotational freedom on the time scale of the fluorescence measurement. Such a randomly oriented probe would have equal x- and y-polarization components and result in a polarization angle of 45°. The 3° difference between the observed ϕ of 48° and the predicted 45° for a disordered probe is most likely a systematic error introduced by the instrumentation and optics. In contrast, the average angle during the event was not unique but distributed between 35° and 59° for any given event (Fig. 4*C Lower*). A gap in the histogram for polarization angles during the event must exist between 45° and 50° because this was the range of observed angles before the event, and for an event to be scored there must have been a change in angle.

How might one interpret ϕ, the polarization angle, in terms of myosin motor function? The actomyosin cycle is viewed as beginning with myosin initially detached from, or weakly bound to actin, and having the products of MgATP hydrolysis in the active site (i.e., MgADP and Pi) (2, 3). This state should be characterized by significant rotational freedom of the myosin-catalytic (4, 15) and light chain domains, translating into the average 48° polarization angle observed before a polarization event. In contrast, a recent EPR study by Baker *et al.* (14) suggests that the weak binding state in skinned scallop fibers is populated by myosin having a light chain domain that is equally distributed between two distinct angular orientations relative to the fiber axis. It is possible that in the fiber, myosin within a thick filament is constrained by intramolecular interactions so that the light chain domain adopts these conformations. However, monomeric myosin adhered to the motility surface assay will be free of these constraints and should exhibit significant rotational freedom, as suggested by the 48° polarization angle.

The powerstroke is generated by myosin first attaching to actin in a strongly bound, prepowerstroke state followed by rotation of the light chain domain, with the powerstroke being coupled to the release of products from the active site. If both the strongly bound pre- and postpowerstroke states are characterized by distinct preferred orientations of the myosin light chain domain relative to the actin filament (14), then polarization events should be biphasic (case 1, Fig. 5). However, only a single preferred angular orientation could be detected. It is still possible that a short-lived, strongly bound prepowerstroke state does occur but that the time resolution of our detection system (10 ms) cannot resolve this state. An alternate hypothesis (case 2, Fig. 5) is that during the strongly bound prepowerstroke state, the light chain domain or the probe itself on the RLC is relatively mobile and thus cannot be resolved from the previous weakly bound state. Once the powerstroke is complete and MgADP has been released from the active site, the myosin will remain attached to actin in a rigor conformation waiting for the next MgATP, as suggested by the prolonged event durations at low MgATP (see Table 1). This rigor conformation is presumably the preferred angular orientation observed during the polarization transient. The fact that this final position at the end of the powerstroke is not unique but ranges between 35° and 59° could reflect the static disorder reported for the rigor conformation from recent EPR studies (14) but most likely is the angle at which randomly adhered myosin has to reach out and attach to actin. Rigor controls, in which labeled myosin was allowed to interact with actin in the absence of MgATP, showed a similar wide range of preferred angles even though no polarization transients were observed (data not shown). The fact that myosin can attach to actin at any angle should have resulted in a range of ϕ between 0° and 90°. We have not corrected for the effects of potential fluorophore wobble on the RLC which would narrow the effective range of detectable orientations (29).

These polarization data from a single myosin molecule provide direct evidence that myosin adopts at least two distinct

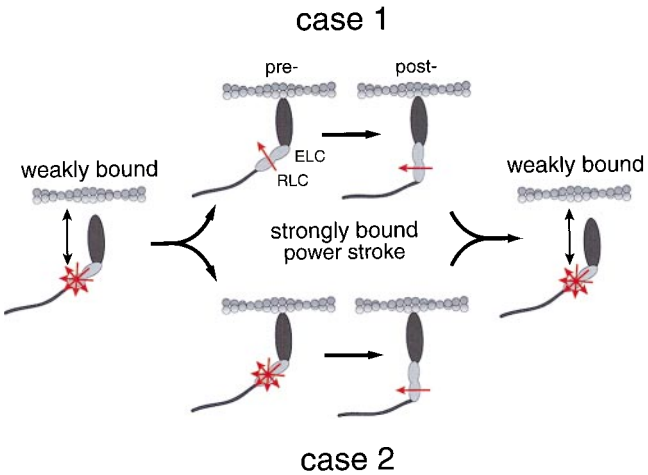

FIG. 5. Illustration of the myosin powerstroke and two scenarios to explain the observed single fluorophore polarization data. See text for explanation. The fluorophore emission dipole on the RLC is depicted as an arrow on the myosin light chain domain with the essential light chain (ELC) also indicated. The multiple red arrows represent a dipole that has significant rotational freedom either caused by rotational freedom of the probe on the myosin molecule or by the probe being relatively fixed to the myosin molecule and that the myosin itself is free to rotate. The weakly bound state, characterized by rapid myosin attachment to and detachment from actin, is indicated by a small vertical two-headed arrow.

conformational states during its cyclic interaction with actin, i.e., a disordered state, presumably the weak binding state, and an ordered state having a definite polarization angle, reflecting the strong binding state after the powerstroke. Although a disordered-to-ordered transition has been assumed in the past (4, 15), the identification of these two states has relied on ensemble averages from solution biochemistry or skinned muscle fiber studies (30). These data thus confirm the presence of such orientational states through fluorophore polarization changes in a single myosin molecule as it undergoes the transition in real-time between the weak to strong binding conformations. However, to detect the powerstroke swing angle using the present technique, molecular biological manipulations may be necessary to generate myosin molecules that possess long-lived prepowerstroke states so that the actual powerstroke can be resolved.

We thank John Corrie for supplying the 6-IATR, Guillermina Waller for preparing the labeled RLC and myosin, the University of Vermont Muscle Club for many stimulating conversations and suggestions, Paul Millman, Dick Stewart, and Jay Reichman at Chroma Technologies for their expert assistance in the design and manufacturing of all filters and dichroic mirrors used in this system, Erwin Deutsch for his microscope expertise, and Shuming Nie for his assistance in the initial design of the instrument. We would like to dedicate this publication to the memory of Dr. Fredric S. Fay, both mentor (D.M.W.) and collaborator (K.T.). His innovative approaches to digital fluorescence spectroscopy inspired numerous investigators to push the limits of fluorescence detection. Fred, we hope we did you proud! This work was supported by grants from the National Science Foundation MRI-9724442, National Institutes of Health AR42231, and a private donation from Irving and Helen Cohen (to D.M.W.), postdoctoral fellowship from the American Lung Association (to A.-M.L.), National Institutes of Health (to K.T. and S.L.), and National Institutes of Health AR44219 (to C.B.).

1. Huxley, A. F. (1957) *Prog. Biophys.* **7,** 255–318.
2. Lymn, R. W. & Taylor, E. W. (1971) *Biochemistry* **10,** 4617–4624.
3. Eisenberg, E., Hill, T. L. & Chen, Y. (1980) *Biophys. J.* **29,** 195–227.
4. Cooke, R., Crowder, M. S. & Thomas, D. D. (1982) *Nature (London)* **300,** 776–778.
5. Cooke, R. (1986) *CRC Crit. Rev. Biochem.* **21,** 53–118.
6. Rayment, I., Rypniewski, W. R., Schmidt-Base, K., Smith, R., Tomchick, D. R., Benning, M. M., Winkelmann, D. A., Wesenberg, G. & Holden, H. M. (1993) *Science* **261,** 58–65.
7. Rayment, I., Holden, H. M., Whittaker, M., Yohn, C. B., Lorenz, M., Holmes, K. C. & Milligan, R. A. (1993) *Science* **261,** 50–58.
8. Huxley, H. E. (1969) *Science* **164,** 1356–1366.
9. Block, S. M. (1996) *Cell* **87,** 151–157.
10. Irving, M., St. Claire, A. T., Sabido-David, C., Craik, J. S., Brandmeier, B., Kendrick-Jones, J., Corrie, J. E. T., Trentham, D. R. & Goldman, Y. E. (1995) *Nature (London)* **375,** 688–691.
11. Ling, N., Shrimpton, C., Sleep, J., Kendrick-Jones, J. & Irving, M. (1996) *Biophys. J.* **70,** 1836–1846.
12. St. Claire, A. T. , Ling, N., Irving, M. & Goldman, Y. E. (1996) *Biophys. J.* **70,** 1847–1862.
13. Berger, C. L., Craik, J. S., Trentham, D. R., Corrie, J. E. T. & Goldman, Y. E. (1996) *Biophys. J.* **71,** 3330–3343.
14. Baker, J. E., Brust-Mascher, I., Ramachandran, S., LaConte, L. E. W. & Thomas, D. D. (1998) *Proc. Natl. Acad. Sci. USA* **95,** 2944–2949.
15. Berger, C. L. & Thomas, D. D. (1994) *Biophys. J.* **67,** 250–261.
16. Nie, S., Chiu, D. T. & Zare, R. N. (1994) *Science* **266,** 1018–1021.
17. Trybus, K. M., Waller, G. S. & Chatman, T. A. (1994) *J. Cell Biol.* **124,** 963–969.
18. Trybus, K. M. & Chatman, T. A. (1993) *J. Biol. Chem.* **268,** 4412–4419.
19. Warshaw, D. M., Desrosiers, J. M., Work, S. S. & Trybus, K. T. (1990) *J. Cell Biol.* **111,** 453–463.
20. Guilford, W. H., Dupuis, D. E., Kennedy, G., Wu, J., Patlak, J. B. & Warshaw, D. M. (1997) *Biophys. J.* **72,** 1006–1021.
21. Dupuis, D., Guilford, W. H., Wu, J. & Warshaw, D. M. (1997) *J. Muscle Res. Cell Motil.* **18,** 17–30.
22. Funatsu, T., Harada, Y., Tokunaga, M., Saito, K. & Yanagida, T. (1995) *Nature (London)* **374,** 555–559.
23. Dickson, R. M., Norris, D. J., Tzeng, Y.-L. & Moerner, W. E. (1996) *Science* **274,** 966–969.
24. Vale, R. D., Funatsu, T., Pierce, D. W., Romberg, L., Harada, Y. & Yanagida, T. (1996) *Nature (London)* **380,** 451–453.
25. Nie, S. & Zare, R. N. (1997) *Annu. Rev. Biophys. Biomol. Struct.* **26,** 567–596.
26. Xu, X.-H. & Yeung, E. S. (1997) *Science* **275,** 1106–1109.
27. Harris, D. E. & Warshaw, D. M. (1993) *J. Biol. Chem.* **268,** 14764–14768.
28. Marston, S. B. & Taylor, E. W. (1980) *J. Mol. Biol.* **139,** 573–600.
29. Irving, M. (1996) *Biophys. J.* **70,** 1830–1835.
30. Brenner, B., Schoenberg, M., Chalovich, J. M., Greene, L. E. & Eisenberg, E. (1982) *Proc. Natl. Acad. Sci. USA* **79,** 7288–7291.